

Review

Laser Sources Based on Rare-Earth Ion Doped Tellurite Glass Fibers and Microspheres

Elena A. Anashkina

Federal Research Center Institute of Applied Physics of the Russian Academy of Sciences, 46 Ul'yanov Street, Nizhny Novgorod 603950, Russia; elena.anashkina@ipfran.ru

Received: 6 March 2020; Accepted: 1 May 2020; Published: 11 May 2020



Abstract: In recent years, huge progress has been made in the development of rare-earth ion doped tellurite glass laser sources, ranging from watt- and multiwatt-level fiber lasers to nanowatt level microsphere lasers. Significant success has been achieved in extending the spectral range of tellurite fiber lasers generating at wavelengths beyond 2 μm as well as in theoretical understanding. This review is aimed at discussing the state of the art of neodymium-, erbium-, thulium-, and holmium-doped tellurite glass fiber and microsphere lasers.

Keywords: tellurite fiber laser; tellurite glass fiber; microlaser; microsphere laser; rare-earth ions

1. Introduction

Tellurite glasses (based on tellurium dioxide TeO_2) possess chemical stability, have a broad transmission range of $\sim 0.4\text{--}6\ \mu\text{m}$, high linear refractive index $n \sim 1.8\text{--}2.3$ (against $n \sim 1.4$ for silica and $n \sim 1.5$ for fluoride glasses), high nonlinear refractive index, and relatively low phonon energies ($\sim 700\text{--}900\ \text{cm}^{-1}$) [1–9]. Many compositions are resistant to crystallization. Additionally, by controlling crystallization, tellurite glass ceramics with promising characteristics can be made [1]. Detailed discussion of the physico-chemical properties of tellurite glasses can be found in the literature [1,2]. Current technologies allow creating high-purity low-loss “ultra-dry” tellurite glasses and fibers [8,9], so with allowance for substantial solubility of rare-earth ions, tellurite glass-based rare-earth-doped elements as active media for laser sources seem very attractive [4,10]. Due to the high refractive index n , the stimulated emission cross sections proportional to $(n^2 + 2)^2/9n$ for tellurite glasses are $\sim 1.5\text{--}2$ times higher than for silica and fluoride ones [10]. Low phonon energies allow operation in the spectral range well beyond 2 μm , expanding the possibilities of achieving longer wavelength generation in comparison with silica glasses [11,12]. It should be noted that fluoride glasses make it possible to obtain even longer wavelength lasing than tellurite glasses; however, fluoride glasses are less resistant to atmospheric moisture.

In addition to choosing the material of gain medium, when developing photonic devices, considerable attention should be paid to the geometry of active elements. Fibers and microspheres have significant benefits in this respect. Thanks to the exploitation of waveguide light propagation, fiber lasers have advantages such as high efficiency of converting pump energy into radiation energy, efficient heat removal, and high quality of the spatial profile of the laser beam. Cavities for tellurite fiber lasers can be formed by bulk mirrors, reflective coatings deposited on fiber ends, fiber ends themselves, or by their combinations. Additional optical elements such as lenses or beam splitters can be also placed into a laser cavity. An example of a possible fiber laser scheme is shown in Figure 1.

For microsphere-based lasers, which can be used as miniature photonic devices for basic science and many real applications—for example, for sensing [13], a gain medium and a cavity are the same device that is a microresonator with whispering gallery modes (WGMs) [14]. Such microresonators typically have high Q-factors (quality factors) and small optical WGM volumes which make them suitable for constructing narrow linewidth and low threshold microlasers [13,14]. For efficient excitation

of WGMs, evanescent-wave coupling is required. Commonly, coupling can be implemented using a tapered fiber with a waist diameter meeting phase matching conditions [14]. Coupling can be also realized by means of a prism by adjusting the angle of incidence to achieve phase matching [15]. An example of a possible microsphere laser scheme is shown in Figure 2.

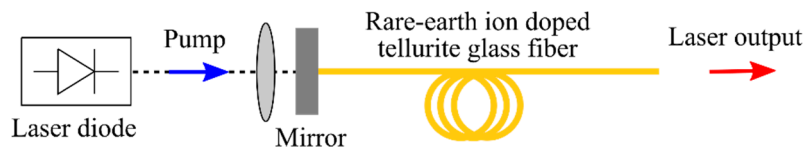


Figure 1. Variant of experimental fiber laser scheme with forward diode pumping using a mirror at the input end and only the fiber end (with Fresnel reflection) at the output as a cavity.

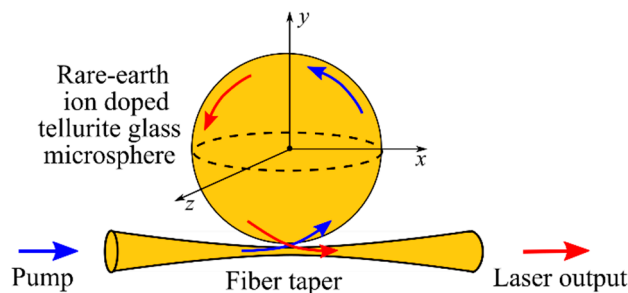


Figure 2. Variant of experimental microlaser scheme with a fiber taper used for both pump coupling and extracting the generated radiation from the microsphere.

In this review, we discuss laser sources utilizing fibers and microspheres based on rare-earth-doped tellurite glasses. Lasing was attained at the radiative transitions of the following ions: Nd^{3+} [16–21], Er^{3+} [22–32], Tm^{3+} [11,12,33–46], and Ho^{3+} [47–56]. In most works on tellurite fiber and microsphere lasers, generation was achieved in a continuous wave (CW) regime. For tellurite fiber lasers, several works were devoted to pulsed generation including via Q-switch [28,38,48] or pulsed pump [12]. The generation of ultrashort pulses via mode-locking has not been reported yet for tellurite fiber and microsphere lasers. Note that, in [1] there is the chapter “Lasers Utilising Tellurite Glass-Based Gain Media” [10] on the same topic with references to the research works published in 2015 and earlier. However, since 2015, significant progress has been made in the development of such laser sources, including achieving the watt and multiwatt level of laser radiation near $2\ \mu\text{m}$ [52,53] and attaining generation in the range well above $2\ \mu\text{m}$ in tellurite active elements [11,12]. Significant advances have been also achieved in the theory of such sources [8,11,29,53,56–59]. Therefore, this review is focused on the recent results. Nevertheless, an attempt of summarizing all the data on the reported tellurite glass fiber-based and microsphere-based lasers has also been made.

2. Neodymium

A rare-earth Nd^{3+} ion has an absorption band near 800 nm corresponding to the wavelengths of commercially available laser diodes and Ti:sapphire lasers [10]. Therefore, these laser sources are widely used for pumping Nd-doped gain media including tellurite glass based ones. Under pumping at a wavelength near 800 nm, Nd^{3+} ions are excited to the (${}^4\text{F}_{5/2}$, ${}^2\text{H}_{9/2}$) states from the ground level ${}^4\text{I}_{9/2}$ via the ground state absorption. Next, rapid relaxation from short-lived (${}^4\text{F}_{5/2}$, ${}^2\text{H}_{9/2}$) states to the upper laser level ${}^4\text{F}_{3/2}$ occurs due to non-radiative multiphonon decay. Furthermore, the emission band of Nd^{3+} peaking at about 1060 nm can be observed due to the ${}^4\text{F}_{3/2} \rightarrow {}^4\text{I}_{11/2}$ transition. A simplified scheme of Nd^{3+} energy levels is shown in Figure 3.

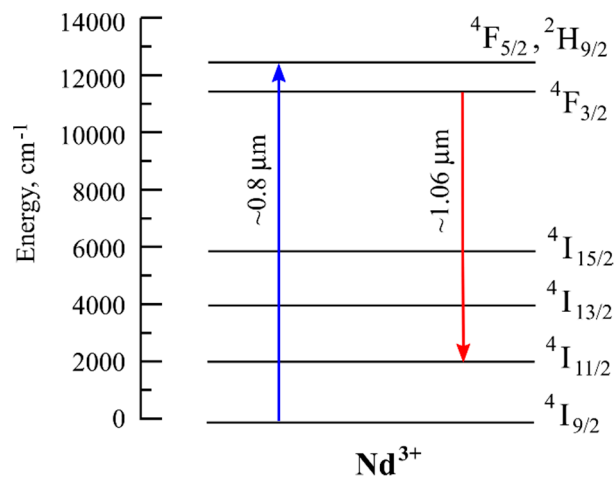


Figure 3. Simplified energy level diagram for Nd-doped tellurite glass.

Note that Nd^{3+} ions can also be pumped at shorter wavelengths. For example, the first tellurite bulk glass-based laser operating near 1060 nm using Nd-doped sample pumped by an Argon laser at 514.5 nm was demonstrated in 1978 [60]. However, with the development of Ti:sapphire lasers and laser diodes, other pump sources for Nd-doped gain elements lost relevance.

2.1. Lasing in Nd-Doped Fibers

The first tellurite glass fiber laser was reported in 1994 [16]. A 0.6-m piece of fiber with 76.9TeO₂-15.5ZnO-6.0Na₂O-1.5Bi₂O₃-0.1Nd₂O₃/75TeO₂-20ZnO-5Na₂O core/cladding glass compositions was pumped by a Ti:sapphire laser at 818 nm. The fiber had an elliptical core and the resonator was organized by Fresnel reflection with a coefficient of 11.9% from each fiber end; external mirrors were not used. The slope efficiency for the power output from one end of the fiber was 23% relative to pump power. Assuming equal emission from both ends, the slope efficiency above threshold was estimated to be 46%. The threshold was approximately 27 mW. Laser generation was single-modal for pumping above the threshold, and became multimodal for pumping well above the laser threshold. The maximal output power from one fiber end exceeded 4 mW [16].

2.2. Lasing in Nd-Doped Microspheres

Lasing in the ~1058–1075 nm range in Nd-doped tellurite microspheres using Ti:sapphire lasers for pumping was reported in several research works [17–21]. The first tellurite microlaser was demonstrated in 2002 [17]. Microspheres with diameters ranging from 50 μm to a few hundred μm were produced by melting the end of a glass wire using a Kanthal wire heater [17]. Microspherical resonators were pumped at 800 nm by a Ti:sapphire laser. The pump light was focused to a point slightly shifted from the center of the microsphere. The output laser radiation at ~1.06 μm was collected using a multimode fiber. The microsphere laser with a diameter of 140 μm had an incident pump threshold of 81 mW, but pump coupling was not optimized [17].

In 2003, it was shown that the oscillation wavelengths of a microlasers could be adjustable using quarter wavelength shifted distributed feedback resonators produced on the surface of microspherical samples [18]. Generated wavelengths agreed with the Bragg wavelengths calculated using the known periods of gratings and the effective refractive indices of WGMs. Tapered optical fibers were used for both coupling the pump light and extracting the output radiation. The threshold of the laser based on a microsphere with a Q-factor of $\sim 10^5$ was lower than 40 mW. Single-mode and multimode generation was observed in the ~1058–1075 nm range for different sphere diameters of ~70–180 μm [18].

Air-bubble-containing Nd-doped tellurite glass microspheres were produced and investigated [21]. The localized laser heating technique was applied for sample fabrication. When the edge part of the microspherical sample with a diameter of 20 μm containing an air bubble with a diameter of

1.6 μm was pumped, periodical spectral peaks were generated. These peaks corresponded to WGMs. However, when the bubble position was pumped, not only WGMs but also a continuous range of other wavelengths were excited. It was shown that the introduction of an air bubble into the microresonator led to “non-WGMs excitation”, reducing the threshold [21]. The lowest reached lasing threshold was 0.034 mW for an air-bubble-containing 4- μm microsphere, which agreed with numerical estimations [21].

3. Erbium

A rare-earth Er^{3+} ion has an absorption band near 980 nm corresponding to the wavelengths of low cost commercial laser diodes which are standard telecom components. Radiation at ~ 980 nm via the ground state absorption from the $^4I_{15/2}$ level excites the $^4I_{11/2}$ level (see Figure 4). After that, the transition from the $^4I_{11/2}$ to the $^4I_{13/2}$ level occurs. For silica glass, due to high phonon energy, the $^4I_{11/2}$ level is depopulated non-radiatively, but for tellurite glasses, the radiative transition near the 2.7–2.8 μm range is possible [61]. After that, the $^4I_{13/2}$ level is populated and lasing in the 1.53–1.6 μm range at the $^4I_{13/2} \rightarrow ^4I_{15/2}$ transition can be attained (see Figure 4). Therefore, tellurite glasses can be used as a gain medium for lasing in the 1.53–1.6 μm range as well as in the 2.7–2.8 μm range. For lasing in the 1.5 μm region, in-band pump by standard laser diodes at 1480 nm or silica fiber lasers can be also used. Er-doped tellurite fibers are promising for L-band lasers and amplifiers [30] due to lower excited-state absorption and higher values of stimulated emission cross-sections in comparison with Er-doped silica fibers for this spectral range [30].

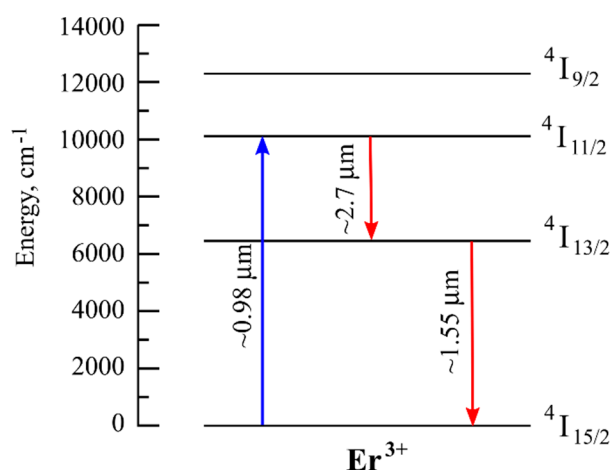


Figure 4. Simplified energy level diagram for Er-doped tellurite glass.

3.1. Lasing in the 1.5 μm Region in Er-Doped Fibers

The first signal amplification and laser oscillation at a wavelength of 1560 nm in Er-doped tellurite fibers was claimed in [22]. A small-signal gain of 16 dB was achieved when a pump power was 130 mW and a pump wavelength was 978 nm. Lasing with a slope efficiency of 0.65% was obtained in a 85-cm fiber. A threshold pump power was 120 mW. A fiber cavity was based on the Fresnel reflection of 12.3% at each end; external mirrors were not used [22]. Since then, Er-doped tellurite fiber lasers have been developed and investigated [23–30].

A CW Er-doped zinc-tellurite fiber laser was recently reported in [29]. A single-mode generation was attained in a 20-cm long piece of fiber with single-mode 975-nm diode pumping. The pump beam was coupled into the core of the fiber using a beam splitter put into a laser cavity which was formed by two aspheric lenses. Laser radiation at 1555 nm was extracted through the beam splitter [29].

L-band wavelength-tunable CW Er-doped tellurite fiber lasers were reported in [30]. Lasing tunable in the 1589–1627 nm range was obtained in the 3-m long fiber made of $\text{TeO}_2\text{-ZnO-La}_2\text{O}_3$ glass. A fiber laser with a maximum output power of 2.5 W at a wavelength of 1570 nm was used as a pump

source [30]. A laser cavity contained a mirror with a high reflectivity, a fiber coupler, a wavelength division multiplexer, an active tellurite fiber, a collimation lens, and diffraction grating. The wavelength tuning was realized with the Littrow configuration [30].

Self-Q-switching behavior of Er-doped tellurite microstructured fiber lasers was reported in [28]. Using a 1480-nm pump with a power of 705 mW, output 282-ns laser pulses with a repetition rate of 1.14 MHz at 1558 nm were obtained in the 14-cm piece of the active fiber using a linear cavity. The maximum average power was 316 mW. The slope efficiency of 72.6% was reached before the saturation. The authors explained the self-Q-switching behavior by the reabsorption originating from the ineffectively pumped part of the Er-doped tellurite microstructured fiber [28].

A high-performance Ce/Er co-doped tellurite fiber laser and a fiber amplifier dual-wavelength pumped at 980 nm and 1480 nm were presented in [23]. A 22-cm long piece of gain fiber in a fiber ring laser configuration was used to generate radiation with a tuning range of 83 nm (from 1527 to 1610 nm). The addition of Ce³⁺ co-doping with Er³⁺ was used for a resonant transfer to Ce (the ²F_{5/2} → ²F_{7/2} energy transition) from Er (the ⁴I_{11/2} → ⁴I_{13/2} energy transition), which reduced excited state absorption from the ⁴I_{11/2} level of Er and improved the gain characteristics at ~1.6 μm [23].

3.2. On the Possibilities of Lasing in the 2.7–2.8 μm Region in Er-Doped Fibers

Luminescence in the 2.7–2.8-μm region at the ⁴I_{11/2} → ⁴I_{13/2} energy transition in tellurite glasses was first observed in [62] and was later reported by various research groups both, in glasses and in fibers [61,63–67]. However, master oscillators or amplifiers at 2.7–2.8 μm based on Er-doped tellurite glass fibers or other tellurite glass optical elements have not been published in refereed journals yet, but studies in this area are being conducted. The first reason for the absence of such coherent light sources is associated with high absorption by OH[−] groups in the considered range. The next reason is that the lifetime τ₃ of level ⁴I_{11/2} is much less than the lifetime τ₂ of level ⁴I_{13/2} due to moderate phonon energy (~900 cm^{−1} for tungsten-modified tellurite glasses and ~750 cm^{−1} for zinc-modified tellurite glasses [1]). For zinc-tellurite glasses, τ₃ is about 200–300 μs [29,61,67] but for tungsten-tellurite glasses τ₃ is about 100 μs [8], whereas τ₂ reaches a few ms for different glass compositions [29,61]. Under continuous wave (CW) pumping at the ⁴I_{15/2} → ⁴I_{11/2} transition, this leads to high population of the ⁴I_{13/2} level and small population of the ⁴I_{11/2} level. A possible way to solve the first challenge is to synthesize high-quality “ultra-dry” TeO₂ glasses [8]. To overcome successfully the second challenge and effectively populate the upper level ⁴I_{11/2}, different paths shown schematically in Figure 5 were proposed. These include:

1. Using heavy Er³⁺ concentrations to provide a significant up-conversion rate (⁴I_{13/2} + ⁴I_{13/2} → ⁴I_{9/2} + ⁴I_{15/2}) (see Figure 5a) [61,66].
2. Using pulsed pumping with a duration of the order of τ₃ and a low enough repetition rate (<1/τ₂) (see Figure 5b) [8].
3. Using dual-wavelength cascade laser schemes at two consecutive radiative transitions ⁴I_{11/2} → ⁴I_{13/2} and ⁴I_{13/2} → ⁴I_{15/2} at 1.56 and 2.8 μm, respectively, see Figure 5c [29].
4. Using two-color pumping with the first pump wavelength of 980 nm (⁴I_{15/2} → ⁴I_{11/2}) or 1.56 μm (⁴I_{15/2} → ⁴I_{13/2}) and the second pump wavelength of 1.7 μm (⁴I_{13/2} → ⁴I_{9/2}) (see Figure 5d) [59].

Regarding the first way, it was proposed to effectively depopulate the level ⁴I_{13/2} and populate the level ⁴I_{11/2} exploiting energy transfer up-conversion processes [61]. It was found experimentally that energy transfer rate parameters strongly depend on Er³⁺ ion concentration [61]. The higher the Er³⁺ content, the larger up-conversion rate is [61]. On the basis of experimental data, it was calculated that for Er³⁺ concentration >1.2·10²¹ cm^{−3} (or Er₂O₃ ~2.65 mol. % for zinc-tellurite glass) and OH[−] concentration equal to zero, a population inversion could be achieved for a pump intensity over 87 kW/cm² at 976 nm [61]. The first theoretical analysis of ultrashort pulse amplification in the 2.7–3 μm range under diode pumping at 975 nm was performed in [66]. The opportunity of obtaining pulses with the duration shorter than 100 fs and the energy of order 10 nJ (with gain of ~20 dB) was shown

numerically for fibers manufactured from high-quality $\text{TeO}_2\text{-ZnO-Na}_2\text{O-La}_2\text{O}_3$ glasses with Er^{3+} concentration of 10^{21} cm^{-3} in the core and a low concentration of OH^- groups [66].

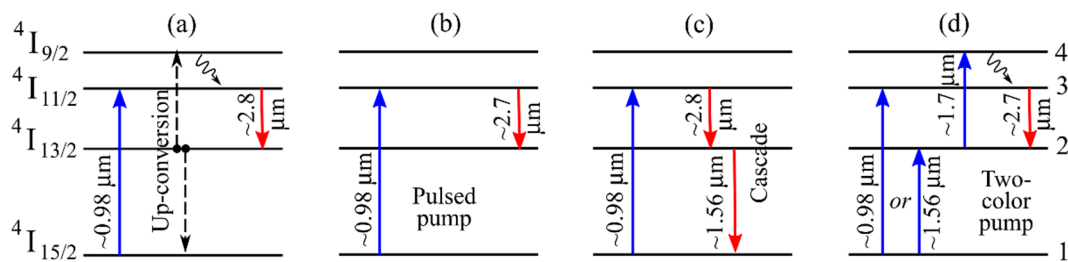


Figure 5. Schematic of different ways of effective population of the $4I_{11/2}$ level of Er^{3+} ions in tellurite glasses. (a) 1. Up-conversion for very high Er^{3+} ion concentrations. (b) 2. Pulsed pump. (c) 3. Dual-wavelength cascade lasing. (d) 4. Two-color pump.

As concerns the second way, a possibility of realizing a diode-pumped gain-switched laser with 100 Hz repetition rate based on specially developed Er-doped single-mode and multi-mode $\text{TeO}_2\text{-WO}_3\text{-La}_2\text{O}_3\text{-Bi}_2\text{O}_3$ glass fibers was proposed and investigated in [8]. When the pump is switched on, the upper laser level $4I_{11/2}$ starts to be populated. The initial population of the $4I_{13/2}$ level is equal to 0. When the pump threshold is attained, laser oscillations start to develop. The corresponding condition is that the signal gain for a cavity round trip is equal to the total losses. The total losses depend on the losses associated with radiation output from the cavity and the losses on optical elements including the fiber losses. When the first pump pulse is applied, the population n_3 of the level $4I_{11/2}$ starts to increase linearly with time. At the moment of spike generation, n_3 decreases and the population n_2 of the level $4I_{13/2}$ increases by the similar value. For the pump duration comparable to τ_3 , the depopulating the upper $4I_{11/2}$ level via spontaneous non-radiative transitions affects significantly. However, the population of metastable level $4I_{13/2}$ with a lifetime of a few ms continues to grow. The generation efficiency becomes reducing and vanishes. Thus, the duration of pump pulses should be of the order of τ_3 . After this, the residual population relaxes from the $4I_{11/2}$ level to the $4I_{13/2}$ level with a characteristic lifetime τ_3 . Relaxation from the $4I_{13/2}$ level to the ground state $4I_{15/2}$ occurs with a characteristic time $\tau_2 \gg \tau_3$. Therefore, the repetition rate of the pump pulses should be chosen low enough so that the vast majority of the ions populating the $4I_{13/2}$ level transits to the $4I_{15/2}$ level by the time the next pump pulse arrives [8].

The third opportunity concerns using dual-wavelength cascade laser schemes at 1.56 μm and 2.8 μm (which was demonstrated for fluoride fiber lasers doped with Er^{3+} ions with 50% slope efficiency at 2.8 μm exceeding the Stokes limit by 15% [68]). The first theoretical analysis of such a scheme for Er-doped tellurite fibers was performed in the paper [29]. A numerical model calibrated to the experimental data (concerning laser generation and amplification at 1.555 μm in $\text{TeO}_2\text{-ZnO-La}_2\text{O}_3\text{-Na}_2\text{O}$ glass fibers doped with 0.24 mol % Er_2O_3 [29]) was developed for simulation and optimization of lasing parameters for schematics with different characteristics [29]. This model can describe single-wavelength laser generation and cascade dual-wavelength laser generation at 1.555 μm and 2.8 μm . It was demonstrated in numerical simulation that for the optimal parameters, the maximum slope efficiency at 2.8 μm at the $4I_{11/2} \rightarrow 4I_{13/2}$ transition can reach $\sim 20\%$. The maximum calculated efficiency at 1.555 μm exceeds 30%.

For the fourth opportunity based on using two-color pumping with the first pump wavelength of 980 nm ($4I_{15/2} \rightarrow 4I_{11/2}$) or 1.56 μm ($4I_{15/2} \rightarrow 4I_{13/2}$) and the second pump wavelength of 1.7 μm ($4I_{13/2} \rightarrow 4I_{9/2}$), the metastable level $4I_{13/2}$ plays a role of a virtual ground state [59]. Under pumping at the first wavelength, the intermediate $4I_{13/2}$ level is populated, and under pumping at the second wavelength, ions from the metastable $4I_{13/2}$ level transit to the short-lived $4I_{9/2}$ level, and after that a non-radiative rapid relaxation observed from the $4I_{9/2}$ level to the level $4I_{11/2}$. The theoretical investigation of lasing at the $4I_{11/2} \rightarrow 4I_{13/2}$ energy transition under two-color pumping based on of the experimentally measured

characteristics of an Er-doped core fiber made of $\text{TeO}_2\text{-ZnO-Na}_2\text{O-La}_2\text{O}_3$ glass with the concentration of Er^{3+} ions of $N_{\text{Er}} = 10^{20} \text{ cm}^{-3}$ was performed in [59]. It was demonstrated numerically that, for the optimized length of the active tellurite fiber, the small-signal gain could be higher than 18 dB and lasing could be attained with a relatively low pump power of several hundreds of mW, whereas the maximum slope efficiency could reach ~40% [59].

Note that for numerical modeling of different schemes of Er-doped and other rare-earth ion-doped fiber lasers, full systems of equations, corresponding approaches and methods for their solution were presented and described in [69–73].

3.3. Lasing in Er-Doped Microspheres

Lasing in Er-doped tellurite microspheres have been demonstrated only at the ${}^4\text{I}_{13/2} \rightarrow {}^4\text{I}_{15/2}$ energy transition using 975-nm pump at the ${}^4\text{I}_{15/2} \rightarrow {}^4\text{I}_{11/2}$ transition [31] and using 1480-nm in-band pump at the ${}^4\text{I}_{15/2} \rightarrow {}^4\text{I}_{13/2}$ transition [32]. Microspheres were fabricated and investigated by the same research group [31,32]. A spin method was applied for fabrication. TeO_2 -based glass was melted in a furnace and after that dropped on a spinning platform. This melted glass was spun out under centrifugal forces and quickly cooled, which led to the formation of microspheres with diameters from a few μm to a few hundred μm by surface tension [31,32]. The Q-factors were estimated to be $10^5\text{--}10^6$ [31,32] and 3×10^6 [32]. A silica fiber taper was used for both, pump coupling and extracting the generated radiation from microspheres. The generation was achieved in the 1560–1610 nm range by adjustment of pump power [31]. By tuning a relative position between the microresonator and the fiber taper and selecting the microsphere size, single-mode as well as multimode lasing in the L-band was reached [31]. The temperature dependence of the wavelength and the laser threshold was also studied in [32]. The wavelength tuning in the ~1606–1608 nm range was experimentally attained and numerically verified with allowance for the thermal expansion of the TeO_2 -based glass. It was shown that the threshold increased with temperature [32].

4. Thulium

A rare-earth Tm^{3+} ion in tellurite glass matrixes has several radiative transitions at the ${}^3\text{F}_4 \rightarrow {}^3\text{H}_6$ transition in the 1.9–2 μm range, at the ${}^3\text{H}_4 \rightarrow {}^3\text{H}_5$ transition near 2.3 μm , and at the ${}^3\text{H}_4 \rightarrow {}^3\text{F}_4$ transition near 1.5 μm as shown in Figure 6. To achieve generation at these transitions, pumping by commercial laser diodes at ~800 nm can be used to excite the ${}^3\text{H}_4$ level from the ground level ${}^3\text{H}_6$ via the ground state absorption at the ${}^3\text{H}_6 \rightarrow {}^3\text{H}_4$ transition. To achieve generation only in the 1.9–2 μm range, in-band fiber laser pump near 1.6 μm can be used effectively.

4.1. Lasing in the 1.9–2 μm Range in Tm-Doped Fibers

The first Tm-doped tellurite fiber laser was reported in [33]. The generation in the 1.88–1.99 μm range was demonstrated in a 32 cm long fiber with core composition of 80 TeO_2 –10 Na_2O –10 ZnO mol % co-doped with 1.5 wt % Yb_2O_3 and 1.0 wt % Tm_2O_3 , and the cladding composition of 75 TeO_2 –10 Na_2O –15 ZnO mol %. The cavity of the laser was formed by a high reflectivity mirror at the pumped end as well as Fresnel reflection of 12% at the opposite output fiber end. Tellurite fibers were in-band pumped by an Er/Yb co-doped silica fiber laser generating in the 1570–1610 nm range. The maximum obtained slope efficiency was 76%. This value was similar to the 82% Stokes limit. The maximum output power of 280 mW was a record one for tellurite fiber lasers [33].

In the further studies of Tm-doped tellurite fiber lasers, an increase in output power to ~0.4 W with in-band pump [40] and to ~0.5 W [36] and 1.12 W [35] with laser diode pump at ~0.8 μm was obtained. A watt level CW lasing at 1937 nm was reached from a specially designed highly Tm-doped double-clad fiber made of tungsten-tellurite glass [35]. The pumped end of the 40-cm long fiber was coated with a dielectric thin film, which was highly reflective for a laser wavelength in the range near 1950 nm and antireflective for a pump wavelength in the range near 800 nm. This coating was used as the first mirror of the laser cavity. As the second mirror of the laser cavity at the output, the fiber

end with ~13% Fresnel reflection was used. The slope efficiency was 20%, and the optical-to-optical efficiency of 16% was reached relative to the absorbed pump power [35].

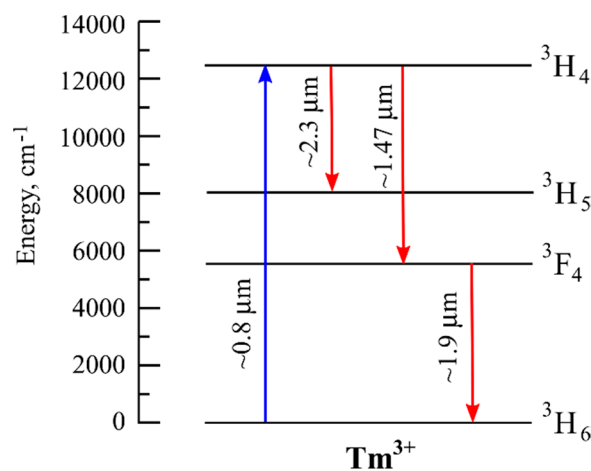


Figure 6. Simplified energy level diagram for Tm-doped tellurite glass.

The first passively Q-switched Tm³⁺-doped tellurite fiber laser was reported in [38]. A semiconductor saturable absorber mirror (SESAM) as well as a carbon nanotubes (CNTs) inserting separately into the fiber laser cavity were used as saturable absorbers to obtain Q-switching. Pulsed lasing at a 1.86 μm without any self-mode-locking effects was observed in a piece of 9-cm long tellurite fiber pumped in-band at 1.59 μm. A CNT Q-switched laser generated 860-ns pulses with an average power of 84 mW, while a SESAM Q-switched laser generated 516-ns pulses with an average power of 21 mW. Pulse energies were 736 nJ and 193 nJ for CNT- and SESAM-based configuration, respectively [38].

The transition from supercontinuum generation to 1.887 μm CW lasing in a Tm-doped tellurite microstructured fiber pumped by a femtosecond fiber laser system at 1.56 μm was observed for the first time in [37]. This transition occurred when varying pulse duration of the pump laser from 290 fs to 3.47 ps. The microstructured 20-cm long fiber made of Tm-doped 78TeO₂-5ZnO-12Na₂CO₃-5Bi₂O₃ glass had a “wagon wheel” cross-section with a solid core surrounded by six air holes. With a decrease in the pump pulse duration from 3.4 ps to 1.3 ps, the threshold of the fiber laser operating at 1887 nm monotonically decreased from 232 mW to 216 mW. The corresponding slope efficiency varied in the 10.2–14.8% range [37].

4.2. Lasing near 2.3 μm in Tm-Doped Fibers

Achieving laser generation at the ³H₄ → ³H₅ transition near 2.3 μm is a more complicated problem than at the ³F₄ → ³H₆ transition in the 1.9–2 μm range, due to the lifetime of the ³H₄ energy level is 10 times shorter than the lifetime of the ³F₄ energy level (~0.3 ms against ~3 ms [74]), and the stimulated emission cross-section at ~2.3 μm is smaller than the stimulated emission cross-section in the 1.9–2 μm range [74]. Therefore, when producing new tellurite glass fibers for lasers operating at 2.3 μm, the quality of the samples should meet more strict requirements than for lasers operating only in the 1.9–2 μm spectral range. It is desirable to fabricate a high-quality low loss fiber, with a very low content of OH⁻ groups. In addition, the concentration of Tm³⁺ ions should be selected carefully. On the one hand, heavy concentrations lead to shorter pump absorption lengths, consequently, to less impact of losses. On the other hand, for heavy concentrations, the cross-relaxation process (³H₄ + ³H₆ → ³F₄ + ³F₄) becomes significant and contributes to depopulation of the energy level ³H₄. Note that for laser generation at the ³F₄ → ³H₆ energy transition, cross relaxation is a helpful process (due to increasing the population of the ³F₄ level), but for generation at the ³H₄ → ³H₅ transition it is parasitic (due to decreasing the population of the ³H₄ level). Therefore, for generating in the ~2.3 μm spectral range, particular attention should be paid to the parameters of glass. As in the case of generation

at $\sim 2.7 \mu\text{m}$ in Er-doped fibers ('the third opportunity'), the bottleneck problem in Tm-doped fibers with a short lifetime of the upper energy level $^3\text{H}_4$ compared with the underlying level $^3\text{F}_4$ can be solved by cascade lasing at two transitions $^3\text{H}_4 \rightarrow ^3\text{H}_5$ and $^3\text{F}_4 \rightarrow ^3\text{H}_6$. The first experimental demonstration of two-color CW cascade laser generation simultaneously near $2.3 \mu\text{m}$ and $1.9 \mu\text{m}$ in the tellurite $\text{TeO}_2\text{-ZnO-La}_2\text{O}_3\text{-Na}_2\text{O}$ glass fiber with Tm-doped core having a concentration of $5 \times 10^{19} \text{ cm}^{-3}$ was reported in [11]. A theoretical investigation of laser amplification and generation, which is in a very good agreement with the experimental results, was also performed in [11]. A numerical model calibrated against experimental data was used to simulate power scalability at $2.3 \mu\text{m}$ in two-color cascade schematics with optimal characteristics under enlarged pump power. It was simulated that the output power at $2.3 \mu\text{m}$ can exceed 0.6 W for backward 10-W pump. Using the same fiber, experimental ultrabroadband amplification of supercontinuum was also obtained with maximum gain of 7 dB and 30 dB at wavelengths of $2.3 \mu\text{m}$ and $1.9 \mu\text{m}$, respectively [11].

The specific problem of short lifetime of the upper laser level for generation at $\sim 2.3 \mu\text{m}$ can be also solved by using pulsed pump (analogously to 'the second way' of lasing in the $2.7\text{--}2.8 \mu\text{m}$ region in Er-doped fibers). This path to generate laser pulses at $2.3 \mu\text{m}$ in Tm-doped $\text{TeO}_2\text{-ZnO-La}_2\text{O}_3\text{-Na}_2\text{O}$ glass fiber under diode pulsed pump at 794 nm was experimentally realized in [12] by setting 1 ms pump duration and 10 ms interval between pulses.

Tm-doped tellurite glass elements can be also used as gain media in the S-band near $1.47\text{--}1.48 \mu\text{m}$ at the $^3\text{H}_4 \rightarrow ^3\text{F}_4$ transition. The possibility of amplification was demonstrated in several papers including under single wavelength pumping at $\sim 795 \text{ nm}$ [75] as well as under dual-wavelength pumping at 795 nm and 1064 nm [75,76], at 1550 nm and at 1047 nm [76], at 1047 nm and at 1605 nm [77], but laser generation at the $^3\text{H}_4 \rightarrow ^3\text{F}_4$ transition in a Tm-doped tellurite fiber has not been reported yet.

4.3. Lasing in Tm-Doped Microspheres

Tm-doped tellurite microsphere lasers generating only at the $^3\text{F}_4 \rightarrow ^3\text{H}_6$ transition near $1.9 \mu\text{m}$ as well as at two consecutive transitions $^3\text{H}_4 \rightarrow ^3\text{F}_4$ and $^3\text{F}_4 \rightarrow ^3\text{H}_6$ simultaneously near 1.5 and $1.9 \mu\text{m}$ in the cascade scheme were reported in [41–46]. Note that such a cascade two-color generation scheme was not implemented for tellurite fiber lasers.

The first Tm-doped tellurite microsphere laser was presented in 2004 [41] by the same research team that constructed the first Nd-doped tellurite microsphere laser [17]. The Tm-doped tellurite microsphere was produced by melting the end of a wire made of tellurite glass. The microlaser was pumped at 800 nm using a tapered fiber. Generation was obtained simultaneously in the $1.9 \mu\text{m}$ band and in the S-band (near $1.5 \mu\text{m}$). The threshold for the $1.9 \mu\text{m}$ band was lower than for the S-band, and the quantum efficiency for the $1.9 \mu\text{m}$ band increased with pump power above the threshold of the S-band [41].

A single-mode microlaser at $2 \mu\text{m}$ pumped by a 973 nm Ti:sapphire laser was demonstrated from a highly Tm-doped tellurite glass microsphere with a diameter of $25 \mu\text{m}$ [42]. Fiber taper was used for pump coupling and laser signal outputting. Note that in the theoretical study of $2\text{-}\mu\text{m}$ lasing in Tm-doped microspheres presented in [57], the obtained numerical results agreed with the experimental ones [42].

A Tm/Ho co-doped tellurite glass microsphere laser at $\sim 1.47 \mu\text{m}$ was implemented at the $^3\text{H}_4 \rightarrow ^3\text{F}_4$ energy transition of the Tm^{3+} ion [46]. Ho^{3+} was co-doped to Tm^{3+} to reduce the population of the long-lived $^3\text{F}_4$ state of the Tm^{3+} ion through a resonant energy transfer process. Using a CO_2 laser, microspheres with diameters ranging from several μm to several hundred μm were produced. Both $\sim 802 \text{ nm}$ pump light of a laser diode and the lasing emission were efficiently guided through a silica tapered fiber. Multimode lasing near $1.47 \mu\text{m}$ as well as single-mode lasing at 1494.9 nm were demonstrated [46].

Recently, laser generation at $1.9 \mu\text{m}$ and visible light of red and green emissions in Tm/Er co-doped tellurite glass microspheres were reached at pumping by 1550 nm broadband amplified spontaneous emission source [45]. Adjusting the relative position between the microsphere and the tapered fiber,

a single-mode microlaser was observed. The output power was 210 nW for the laser wavelength of 1891.63 nm, the line width was 0.18 nm, and the ratio of the side-mode suppression was 12.04 dB. The threshold pump power coupled into a microspherical resonator was 1.5 mW. Single-mode and multimode lasing was observed by adjusting the coupling [45].

A theoretical investigation of multi-color CW lasing in Tm-doped tellurite glass microspheres pumped at a wavelength near 0.8 μm was presented in [58]. The numerical model was based on solving a system of equations for intracavity field amplitudes for all fundamental WGMs in the gain bands and rate equations using experimental parameters of Tm-doped tellurite glass. It was shown that, depending on Q-factors and pump powers, different generation regimes can be attained including single-color lasing at a wavelength of ~ 1.9 μm , two-color lasing at wavelengths of ~ 1.9 and 1.5 μm and at ~ 1.9 and 2.3 μm , and three-color lasing at wavelengths of ~ 1.9 and 1.5 and 2.3 μm [58]. However, unlike fiber lasers generated at 2.3 μm [11,12], tellurite microlasers at 2.3 μm have not yet been reported. The theoretical results obtained in [58] agreed with the experimental data reported in [41,43].

5. Holmium

Generation in the 2–2.1 μm range can be attained with Ho^{3+} ion at the ${}^5\text{I}_7 \rightarrow {}^5\text{I}_8$ transition, which is shown in Figure 7. However, unlike Nd^{3+} , Er^{3+} , and Tm^{3+} ions considered above, Ho^{3+} has no absorption bands corresponding to commercial low cost laser diodes at wavelength of ~ 800 nm or ~ 980 nm. In-band pumping at the ${}^5\text{I}_8 \rightarrow {}^5\text{I}_7$ transition can be implemented by Tm-doped silica fiber lasers. Pumping at the ${}^5\text{I}_8 \rightarrow {}^5\text{I}_6$ transition near 1.1 μm by a specially designed fiber laser, including Raman lasers, can be also reasonable. Another way is to use co-doping with a sensitising ion to provide useful absorption bands. A popular ion for co-doping is Tm^{3+} pumped near 800 nm by a laser diode. In this case, a so-called ‘two-for-one’ cross-relaxation process of Tm ions can be utilized (when an excited ion at the ${}^3\text{H}_4$ level transfers a part of its energy to an ion at the ground state, and after that both ions populate the intermediate ${}^3\text{F}_4$ level), so the energy transfer from the ${}^3\text{F}_4$ level of the Tm^{3+} ion to the ${}^5\text{I}_7$ level of the Ho^{3+} ion can be very efficient. Co-doping with Yb^{3+} ions allows pumping by laser diodes at 980 nm. Nd^{3+} ions can be also used as sensitizers, which was recently proposed and demonstrated for a 795-nm diode pumped Nd/Ho co-doped tellurite fiber laser [51].

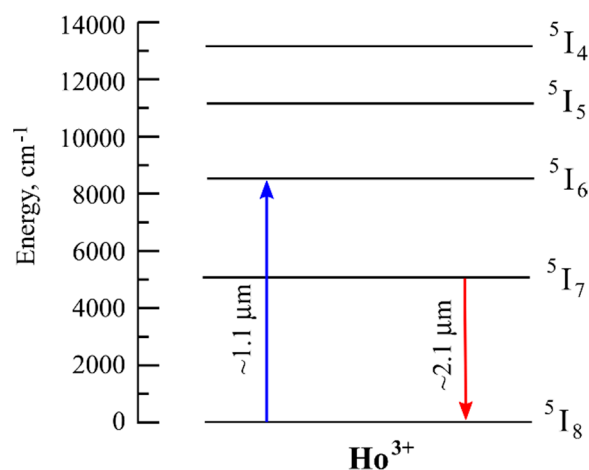


Figure 7. Simplified energy level diagram for Ho-doped tellurite glass.

5.1. Lasing in Ho-Doped Fibers

CW lasing at 2.1 μm from a Tm/Ho/Yb triply-doped tellurite fiber was presented in [48]. The generation at the ${}^5\text{I}_7 \rightarrow {}^5\text{I}_8$ transition of Ho ions was observed. Using an Yb-doped silica fiber laser at 1.1 μm as a pump source, it was suggested to co-dope tellurite gain fiber for sensitization by both Tm and Yb ions to provide a more efficient energy transfer path in comparison with sensitization by Yb alone. For a 17-cm piece of active fiber and a cavity with a reflectivity of 60–99%, the 15-mW

threshold was observed. The slope efficiency was 25%. A maximum output power of 60 mW was obtained for a launched pump power of 270 mW which corresponded to an optical-to-optical efficiency of 22%. The same authors reported CW and Q-switch lasing from a Tm/Ho/Yb co-doped tellurite fiber pumped at $\sim 1.6 \mu\text{m}$ by an Er/Yb silica fiber laser (the Yb^{3+} ions were added with other experiments in mind; they have no absorption at wavelengths $>1.1 \mu\text{m}$ and therefore were not thought to play an active role) [48]. For CW operation, the slope efficiency was 62% and the threshold was 100 mW; the maximum output power was 160 mW. Mechanical Q-switching resulted in pulses with an energy of 0.65 μJ , and a duration of 160 ns at a repetition rate of 19.4 kHz was achieved [48].

A watt-level generation at 2051 μm with a slope efficiency of 31.9% was attained with 50-cm long Ho/Tm co-doped $50\text{TeO}_2\text{-}25\text{GeO}_2\text{-}3\text{WO}_3\text{-}5\text{La}_2\text{O}_3\text{-}3\text{Nb}_2\text{O}_5\text{-}5\text{Li}_2\text{O-}9\text{BaF}_2$ glass fiber pumped by an Er-doped fiber laser at 1560 nm [52]. The threshold power was 0.336 W. The maximum output power was 0.993 W when the pump power was 2.97 W [52].

A multiwatt laser output from a 30-cm piece of microstructured Ho-doped fluorotellurite fiber was recently reported in [53]. A Tm-doped silica fiber laser at 1980 nm was used for pumping. When the threshold pump power was 61.8 mW, lasing at 2067 nm started. The highest unsaturated output laser power of $\sim 8.08 \text{ W}$ was achieved for a 10.56-W pump [53]. The slope efficiency was approximately 77%. Numerical simulation of lasing for experimental parameters was also performed by solving the rate equations and propagation equations. The experimental and numerical results were in a good agreement [53].

5.2. Lasing in Ho-Doped Microspheres

A single-mode Ho-doped tellurite glass microsphere laser directly pumped by a fiber laser at 1150 nm was studied in [55]. The lasing at $\sim 2 \mu\text{m}$ with a low-threshold of 342 μW was achieved. The dynamic characteristics of the microsphere laser were also studied theoretically by considering rare-earth ion spectroscopy, the rate equation of the rare-earth energy level, and the light-matter interactions in the microsphere [55].

The fabrication and characterization of microsphere lasers operating at wavelengths near 2.1 μm was reported in [54]. A Tm/Ho co-doped tellurite glass was used to produce hundreds of high quality microspheres simultaneously (with Q-factors reaching 10^6) by a droplet method [54]. Using a laser diode at 808 nm as a pump source, single-mode, and multimode generation was observed as the pump power was increased beyond a threshold of 887 μW . The maximum laser power reached 105.8 nW and the longest wavelength of the laser radiation reached 2099.52 nm for the sphere with a diameter of 59.52 μm . It was also demonstrated that a microlaser could be thermally tuned [54].

6. Opportunities for Other Rare-Earth Ions

In addition to the rare-earth ions discussed above, using other rare-earth ions for the development of tellurite glass based laser elements was investigated and discussed. There are a lot of works reporting the production of tellurite glass samples doped with Yb^{3+} [78,79], Dy^{3+} [67,80,81], Pr^{3+} [81–83], Eu^{3+} [81,84], Tb^{3+} [81,85], and Sm^{3+} [85,86] and study of their luminescent and other optical, physical, and chemical properties. However, we could not find information about laser generation in tellurite glass fibers or microspheres operating at the radiative transitions of these rare-earth ions.

7. Summary

The state of the art of tellurite glass fiber and microsphere lasers has been reviewed. It has been demonstrated that high-quality rare-earth doped tellurite fibers are promising novel gain elements for lasers and amplifiers in the L-band and in the range of 2 μm and well beyond. Tellurite microsphere lasers are also an attractive platform for developing ultracompact, low threshold, narrow linewidth light sources. The main experimental results on tellurite glass fiber lasers and microsphere lasers are summarized in Tables 1 and 2, respectively.

Table 1. Summary of performance of rare-earth doped tellurite glass fiber lasers.

Dopant	Glass Composition	Fiber Length, cm	Pump Laser, Pump Wavelength, nm	CW or Pulsed	Laser Wavelength, nm	Maximum Output Power (or Energy)	Year, Reference
Nd ³⁺	76.9TeO ₂ -6.0Na ₂ O-15.5ZnO-1.5Bi ₂ O ₃ -0.1Nd ₂ O ₃	60	Ti: sapphire, 818	CW	1061	4.2 mW	1994 [16]
Er ³⁺	Not reported	85	Ti: sapphire, 978	CW	1560	2.5 mW	1997 [22]
Er ³⁺ , 0.9-10 ²⁰ cm ⁻³ , Ce ³⁺ , 2.1-10 ²⁰ cm ⁻³	80TeO ₂ -10ZnO-10Na ₂ O	22	Laser diodes, 980&1480	CW	1527–1610	0 dBm (1 mW) @1558 nm	2011 [23]
Er ³⁺ , 8.12-10 ¹⁹ cm ⁻³ , Ce ³⁺ , 1.92-10 ¹⁹ cm ⁻³	79TeO ₂ -13ZnO-8Na ₂ O	10	Laser diodes, 980&1480	CW	~1550	2.6 mW	2012 [24]
Er ³⁺ , 10 ¹⁹ cm ⁻³	TeO ₂ -ZnO-La ₂ O ₃ -Na ₂ O	~220	Laser diode, 974	CW	~1550	<1 mW	2012 [25]
Er ³⁺ , (7500 ppm Er ₂ O ₃)	71TeO ₂ -22.5WO ₃ -5Na ₂ O-1.5Nb ₂ O ₅	5–16	Laser diode, 980	CW	1530–1565	≤−24.39 dBm (≤3.6 μW)	2012 [26]
Er ³⁺ , (Er ₂ O ₃ 5000 ppm)	78TeO ₂ -5ZnO-12Na ₂ CO ₃ -5Bi ₂ O ₃	17	Laser diode, 1480	CW	1561	140 mW	2013 [27]
Er ³⁺ , 10000 ppm	76.5TeO ₂ -6Bi ₂ O ₃ -6ZnO-11.5Li ₂ O	14	Fiber Raman laser, 1480	Pulsed (self-Q-switch)	1558	316 mW	2014 [28]
Er ³⁺ , 10 ²⁰ cm ⁻³	TeO ₂ -ZnO-La ₂ O ₃ -Na ₂ O	20	Laser diode, 975	CW	1555	>100 μW	2019 [29]
Er ³⁺ , 1 wt %	(50–80) TeO ₂ -(10–40) ZnO-(10 – x) La ₂ O ₃ -xEr ₂ O ₃	~300	Fiber laser, 1570	CW	1589–1627	52.4 mW @ 1614 nm	2019 [30]
Tm ³⁺ /Yb ³⁺ (1.5/1.0 wt % Yb ₂ O ₃ /Tm ₂ O ₃)	80TeO ₂ -10ZnO-10Na ₂ O	32	Fiber laser, 1568–1610	CW	1880–1990	280 mW	2008 [33]
Tm ³⁺ /Yb ³⁺ (1.5/1.0 wt % Yb ₂ O ₃ /Tm ₂ O ₃)	80TeO ₂ -10ZnO-10Na ₂ O	22	Fiber laser, 1088	CW	1910–1994	67 mW	2009 [34]
Tm ³⁺ 3.76 × 10 ²⁰ cm ⁻³	60TeO ₂ -30WO ₃ -10La ₂ O ₃	40	Laser diode, 800	CW	1937	1.12 W	2010 [35]
Tm ³⁺ , 1 mol %	60TeO ₂ -30WO ₃ -10La ₂ O ₃	20	Laser diode, 793	CW	~1900	494 mW	2012 [36]
Tm ³⁺ , 5000 ppm	78TeO ₂ -5ZnO-12Na ₂ CO ₃ -5Bi ₂ O ₃	20	Femto-second fiber system, 1560	CW	1887	>6.5 mW	2014 [37]
Tm ³⁺ , 3.76 × 10 ²⁰ cm ⁻³	Not reported	9	Fiber laser, 1590	Pulsed (Q-switch)	1860	84 mW, 736 nJ	2015 [38]
Tm ³⁺ , 1 mol % Tm ₂ O ₃	45GeO ₂ -25TeO ₂ -15PbO-10(La ₂ O ₃ + Al ₂ O ₃)-5(CaO+ SrO+ Li ₂ O)	26	Laser diode, 793	CW	1968	0.75 W	2015 [39]
Tm ³⁺ , 0.5% Tm ₂ O ₃	70TeO ₂ -10BaF ₂ -9.5Y ₂ O ₃ -0.5Tm ₂ O ₃	42.5	Fiber laser, 1570	CW	1887	408 mW	2017 [40]
Tm ³⁺ , 5 × 10 ¹⁹ cm ⁻³	TeO ₂ -ZnO-La ₂ O ₃ -Na ₂ O	~220	Laser diode, 792	CW	2300&1950	1.7 mW @2300 nm, ~40 mW @1950 nm	2018 [11]
Tm ³⁺ , 5 × 10 ¹⁹ cm ⁻³	(86 – x) TeO ₂ -xZnO-4La ₂ O ₃ -10Na ₂ O	30	Laser diode, 794	Pulsed	2300; 2300&1900	A few μW	2019 [12]
Tm ³⁺ /Ho ³⁺ /Yb ³⁺ , (1.5/1.0/1.0 wt % Yb ₂ O ₃ /Tm ₂ O ₃ /Ho ₂ O ₃)	80TeO ₂ -10ZnO-10Na ₂ O	17	Fiber laser, 1088	CW	~2100	60 mW	2008 [47]
Tm ³⁺ /Ho ³⁺ /Yb ³⁺ , (1.5/1.0/1.0 wt % Yb ₂ O ₃ /Tm ₂ O ₃ /Ho ₂ O ₃)	80TeO ₂ -10ZnO-10Na ₂ O	76 79	Fiber laser, 1600 Fiber laser, 1600	CW Pulsed (Q-switch)	2051–2096 ~2100	160 mW 26 mW, 1.3 μJ (train), 0.65 μJ (main pulse)	2008 [48]
Tm ³⁺ /Ho ³⁺ , 1 mol %/0.5 mol %	60TeO ₂ -30WO ₃ -10La ₂ O ₃	7	Laser diode, 793	CW	2046	35 mW	2012 [36]
Ho ³⁺ , 0.75% Ho ₂ O ₃	70TeO ₂ -20BaF ₂ -9.25Y ₂ O ₃ -0.75Ho ₂ O ₃	27	Fiber laser, 1992	CW	2077	161 mW	2015 [49]
Ho ³⁺ , 0.5% Ho ₂ O ₃	60TeO ₂ -30WO ₃ -9.5La ₂ O ₃ -0.5Ho ₂ O ₃	9	Fiber laser, 1940	CW	2040	34 mW	2016 [50]
Nd ³⁺ /Ho ³⁺ , 0.5% Nd ₂ O ₃ /0.5% Ho ₂ O ₃	60TeO ₂ -30WO ₃ -3ZnO-6La ₂ O ₃ -0.5Ho ₂ O ₃ -0.5Nd ₂ O ₃	5	Laser diode, 975	CW	2052	12 mW	2016 [51]
Tm ³⁺ /Ho ³⁺ , Ho ₂ O ₃ : 0.3%mol, Tm ₂ O ₃ : 0.3%mol	50TeO ₂ -25GeO ₂ -3WO ₃ -5La ₂ O ₃ -3Nb ₂ O ₅ -5Li ₂ O-9BaF ₂	50	Fiber laser, 1560	CW	2051	0.993	2017 [52]
Ho ³⁺ , 0.75% Ho ₂ O ₃	70TeO ₂ -20BaF ₂ -9.25Y ₂ O ₃ -0.75Ho ₂ O ₃	30	Fiber laser, 1980	CW	2067	8.08 W	2019 [53]

Table 2. Summary of performance of rare-earth doped tellurite glass microsphere lasers.

Dopant	Glass Composition	Sphere Diameter, μm	Pump Laser, Pump Wavelength, nm	Single-Mode (SM) or Multi-Mode (MM)	Laser Wavelength, nm	Year, Reference
Nd^{3+} , (1 wt % Nd_2O_3)	$70\text{TeO}_2\text{-}20\text{ZnO-}10\text{Li}_2\text{O}$	201 (50-a few hundred)	Ti: sapphire, 800	MM	~ 1060 (1061–1067)	2002 [17]
Nd^{3+} , (0.2 wt % Nd_2O_3)	$75\text{TeO}_2\text{-}20\text{ZnO-}5\text{Na}_2\text{O}$	$\sim 70\text{--}180$	Ti: sapphire, 800	SM and MM	$\sim 1058\text{--}1075$	2003 [18]
Nd^{3+} , (1 mol % Nd_2O_3)	$80\text{TeO}_2\text{-}10\text{K}_2\text{O-}10\text{WO}_3$ air-bubble-containing or solid	$\sim 20\text{--}50$	Ti: sapphire, 810	MM	$\sim 1060\text{--}1070$	2012 [19]
Nd^{3+} , (1 mol % Nd_2O_3)	$80\text{TeO}_2\text{-}10\text{K}_2\text{O-}10\text{WO}_3$	29	Ti: sapphire, 800–810	SM and MM	$\sim 1060\text{--}1070$	2015 [20]
Nd^{3+} , (1 mol % Nd_2O_3)	$80\text{TeO}_2\text{-}10\text{K}_2\text{O-}10\text{WO}_3$ air-bubble-containing or solid	$\sim 4\text{--}200$	Ti: sapphire, 790–817	MM	$\sim 1060\text{--}1070$	2015 [21]
Er^{3+} , ($1.7 \times 10^{20} \text{ cm}^{-3}$)	Not reported	33	975	SM and MM	1560–1610	2003 [31]
Er^{3+}	Not reported	31	1480	SM	$\sim 1606\text{--}1608$	2003 [32]
Tm^{3+} , (0.15% Tm_2O_3)	$74.85\text{TeO}_2\text{-}20\text{ZnO-}5\text{Na}_2\text{O-}0.15\text{Tm}_2\text{O}_3$	104	Ti: sapphire, 800	MM	$\sim 1500\&1900$	2004 [41]
Tm^{3+} , (5 wt %)	Not reported	25	Ti: sapphire, 793	SM	~ 2000	2005 [42]
Tm^{3+} , 0.5 wt % Tm_2O_3	Not reported	Not reported	Ti: sapphire, 793	MM	$\sim 1500\&1900$	2005 [43]
Tm^{3+} , ($4.2 \times 10^{20} \text{ cm}^{-3}$)	$74\text{TeO}_2\text{-}15\text{ZnO-}5\text{Na}_2\text{O-}5\text{ZnCl}_2\text{-}1\text{Tm}_2\text{O}_3$ (mol. %)	30	1504–1629	MM	Centered at ~ 1975	2015 [44]
$\text{Er}^{3+}/\text{Tm}^{3+}$ (0.1/0.2% $\text{Er}_2\text{O}_3/\text{Tm}_2\text{O}_3$)	$68.7\text{TeO}_2\text{-}23\text{WO}_3\text{-}8\text{La}_2\text{O}_3\text{-}0.1\text{Er}_2\text{O}_3\text{-}0.2\text{Tm}_2\text{O}_3$ (mol %)	110	Amplified spontaneous emission source, 1527–1603	SM and MM	~ 1900	2019 [45]
$\text{Tm}^{3+}/\text{Ho}^{3+}$ (0.2/0.8% $\text{Tm}_2\text{O}_3/\text{Ho}_2\text{O}_3$)	$72\text{TeO}_2\text{-}20\text{ZnO-}5.0\text{Na}_2\text{CO}_3\text{-}2.0\text{Y}_2\text{O}_3\text{-}0.8\text{Ho}_2\text{O}_3\text{-}0.2\text{Tm}_2\text{O}_3$	~ 100	Laser diode, 802	SM and MM	~ 1470	2019 [46]
$\text{Tm}^{3+}/\text{Ho}^{3+}$ (1.0/0.7% $\text{Tm}_2\text{O}_3/\text{Ho}_2\text{O}_3$)	$75\text{TeO}_2\text{-}18.3\text{ZnO-}5\text{Na}_2\text{O-}1.0\text{Tm}_2\text{O}_3\text{-}0.7\text{Ho}_2\text{O}_3$	~ 60	Laser diode, 808	SM and MM	~ 2100	2017 [54]
Ho^{3+} , (1 mol % HoF_3)	$72\text{TeO}_2\text{-}20\text{ZnO-}5\text{Na}_2\text{CO}_3\text{-}2\text{Y}_2\text{O}_3\text{-}1\text{HoF}_3$ (in mol %)	~ 42	Fiber laser, 1150	SM	~ 2080	2020 [55]
$\text{Ho}^{3+}/\text{Yb}^{3+}$ (0.2/0.8% $\text{Ho}_2\text{O}_3/\text{Yb}_2\text{O}_3$)	$72\text{TeO}_2\text{-}20\text{ZnO-}5\text{Na}_2\text{CO}_3\text{-}2\text{Y}_2\text{O}_3\text{-}0.8\text{Yb}_2\text{O}_3\text{-}0.2\text{Ho}_2\text{O}_3$	80	Laser diode, 980	SM and MM	$\sim 2065\text{--}2072$	2020 [56]

Funding: The review of microsphere lasers was funded by the Russian Science Foundation, grant no. 18-72-00176. The review of fiber lasers was funded by the Russian Foundation for Basic Research, grant no. 20-03-00874.

Conflicts of Interest: The author declares no conflict of interest.

References

1. El-Mallawany, R.A.H. *Tellurite Glasses Handbook: Physical Properties and Data*; CRC Press: Boca Raton, FL, USA, 2016.
2. Rivera, V.A.G.; Manzani, D. (Eds.) *Technological Advances in Tellurite Glasses*; Springer: Berlin, Germany, 2017; Volume 254. [[CrossRef](#)]
3. Tao, G.; Ebdorff-Heidepriem, H.; Stolyarov, A.M.; Danto, S.; Badding, J.V.; Fink, Y.; Ballato, J.; Abouraddy, A.F. Infrared fibers. *Adv. Opt. Photonics* **2015**, *7*, 379–458. [[CrossRef](#)]
4. Jha, A.; Richards, B.; Jose, G.; Teddy-Fernandez, T.; Joshi, P.; Jiang, X.; Lousteau, J. Rare-earth ion doped TeO₂ and GeO₂ glasses as laser materials. *Prog. Mater. Sci.* **2012**, *57*, 1426–1491. [[CrossRef](#)]
5. Smayev, M.P.; Dorofeev, V.V.; Moiseev, A.N.; Okhrimchuk, A.G. Femtosecond laser writing of a depressed cladding single mode channel waveguide in high-purity tellurite glass. *J. Non-Cryst. Solids* **2018**, *480*, 100–106. [[CrossRef](#)]
6. Yakovlev, A.I.; Snetkov, I.L.; Dorofeev, V.V.; Motorin, S.E. Magneto-optical properties of high-purity zinc-tellurite glasses. *J. Non-Cryst. Solids* **2018**, *480*, 90–94. [[CrossRef](#)]
7. Alazoumi, S.H.; Aziz, S.A.; El-Mallawany, R.; Aliyu, U.S.; Kamari, H.M.; Zaid, M.H.M.M.; Matori, K.A.; Ushah, A. Optical properties of zinc lead tellurite glasses. *Results Phys.* **2018**, *9*, 1371–1376. [[CrossRef](#)]
8. Anashkina, E.A.; Dorofeev, V.V.; Koltashev, V.V.; Kim, A.V. Development of Er³⁺-doped high-purity tellurite glass fibers for gain-switched laser operation at 2.7 μm. *Opt. Mater. Express* **2017**, *7*, 4337–4351. [[CrossRef](#)]
9. Dorofeev, V.V.; Moiseev, A.N.; Churbanov, M.F.; Kotereva, T.V.; Chilyasov, A.V.; Kraev, I.A.; Pimenov, V.G.; Ketkova, L.A.; Dianov, E.M.; Plotnichenko, V.G.; et al. Production and properties of high purity TeO₂–WO₃–(La₂O₃, Bi₂O₃) and TeO₂–ZnO–Na₂O–Bi₂O₃ glasses. *J. Non-Cryst. Solids* **2011**, *357*, 2366–2370. [[CrossRef](#)]
10. Richards, B.D.; Jha, A. Lasers utilising tellurite glass-based gain media. In *Technological Advances in Tellurite Glasses*; Rivera, V.A.G., Manzani, D., Eds.; Springer: Berlin, Germany, 2017; Volume 254, pp. 101–130. [[CrossRef](#)]
11. Muravyev, S.V.; Anashkina, E.A.; Andrianov, A.V.; Dorofeev, V.V.; Motorin, S.E.; Koptev, M.Y.; Kim, A.V. Dual-band Tm³⁺-doped tellurite fiber amplifier and laser at 1.9 μm and 2.3 μm. *Sci. Rep.* **2018**, *8*, 16164. [[CrossRef](#)]
12. Denker, B.I.; Dorofeev, V.V.; Galagan, B.I.; Koltashev, V.V.; Motorin, S.E.; Plotnichenko, V.G.; Sverchkov, S.E. 2.3 μm laser action in Tm³⁺-doped tellurite glass fiber. *Laser Phys. Lett.* **2019**, *16*, 015101. [[CrossRef](#)]
13. Reynolds, T.; Riesen, N.; Meldrum, A.; Fan, X.; Hall, J.M.; Monroe, T.M.; François, A. Fluorescent and lasing whispering gallery mode microresonators for sensing applications. *Laser Photonics Rev.* **2017**, *11*, 1600265. [[CrossRef](#)]
14. He, L.; Özdemir, Ş.K.; Yang, L. Whispering gallery microcavity lasers. *Laser Photonics Rev.* **2012**, *7*, 60–82. [[CrossRef](#)]
15. Strekalov, D.V.; Marquardt, C.; Matsko, A.B.; Schwefel, H.G.; Leuchs, G. Nonlinear and quantum optics with whispering gallery resonators. *J. Opt.* **2016**, *18*, 123002. [[CrossRef](#)]
16. Wang, J.S.; Machewirth, D.P.; Wu, F.; Snitzer, E.; Vogel, E.M. Neodymium-doped tellurite single-mode fiber laser. *Opt. Lett.* **1994**, *19*, 1448–1449. [[CrossRef](#)]
17. Sasagawa, K.; Kusawake, K.; Ohta, J.; Nunoshita, M. Nd-doped tellurite glass microsphere laser. *Electron. Lett.* **2002**, *38*, 1355–1357. [[CrossRef](#)]
18. Sasagawa, K.; Yonezawa, Z.; Ohta, J.; Nunoshita, M. Control of microsphere lasing wavelength using λ/4-shifted distributed feedback resonator. *Electron. Lett.* **2003**, *39*, 1817–1819. [[CrossRef](#)]
19. Kishi, T.; Kumagai, T.; Yano, T.; Shibata, S. On-chip fabrication of air-bubble-containing Nd³⁺-doped tellurite glass microsphere for laser emission. *AIP Adv.* **2012**, *2*, 042169. [[CrossRef](#)]
20. Kishi, T.; Kumagai, T.; Shibuya, S.; Prudenzeno, F.; Yano, T.; Shibata, S. Quasi-single mode laser output from a terrace structure added on a Nd³⁺-doped tellurite-glass microsphere prepared using localized laser heating. *Opt. Express* **2015**, *23*, 20629–20635. [[CrossRef](#)]
21. Kumagai, T.; Kishi, T.; Yano, T. Low threshold lasing of bubble-containing glass microspheres by non-whispering gallery mode excitation over a wide wavelength range. *J. Appl. Phys.* **2015**, *117*, 113104. [[CrossRef](#)]

22. Mori, A.; Ohishi, Y.; Sudo, S. Erbium-doped tellurite glass fibre laser and amplifier. *Electron. Lett.* **1997**, *33*, 863–864. [[CrossRef](#)]
23. Dong, J.; Wei, Y.Q.; Wonfor, A.; Penty, R.V.; White, I.H.; Lousteau, J.; Jose, G.; Jha, A. Dual-Pumped Tellurite Fiber Amplifier and Tunable Laser Using Er³⁺/Ce³⁺ Codoping Scheme. *IEEE Photonics Technol. Lett.* **2011**, *23*, 736–738. [[CrossRef](#)]
24. Lousteau, J.; Boetti, N.G.; Chiasera, A.; Ferrari, M.; Abrate, S.; Scarciglia, G.; Venturello, A.; Milanese, D. Er³⁺ and Ce³⁺ Codoped Tellurite Optical Fiber for Lasers and Amplifiers in the Near-Infrared Wavelength Region: Fabrication, Optical Characterization, and Prospects. *IEEE Photonics J.* **2012**, *4*, 194–204. [[CrossRef](#)]
25. Oermann, M.R.; Ebdorff-Heidepriem, H.; Ottaway, D.J.; Lancaster, D.G.; Veitch, P.J.; Monroe, T.M. Extruded microstructured fiber lasers. *IEEE Photonics Technol. Lett.* **2012**, *24*, 578–580. [[CrossRef](#)]
26. Chillce, E.F.; Narro-García, R.; Menezes, J.W.; Rodriguez, E.; Marconi, D.; Fragnito, H.L.; Barbosa, L.C. Er³⁺-doped micro-structured tellurite fiber: Laser generation and optical gain. In *Optical Components and Materials IX*; International Society for Optics and Photonics: Bellingham, WA, USA, 2012; Volume 8257, p. 82570B. [[CrossRef](#)]
27. Jia, Z.; Li, H.; Meng, X.; Liu, L.; Qin, G.; Qin, W. Broadband amplification and highly efficient lasing in erbium-doped tellurite microstructured fibers. *Opt. Lett.* **2013**, *38*, 1049–1051. [[CrossRef](#)] [[PubMed](#)]
28. Jia, Z.X.; Yao, C.F.; Kang, Z.; Qin, G.S.; Ohishi, Y.; Qin, W.P. Self-Q-switching behavior of erbium-doped tellurite microstructured fiber lasers. *J. Appl. Phys.* **2014**, *115*, 223103. [[CrossRef](#)]
29. Anashkina, E.A.; Andrianov, A.V.; Dorofeev, V.V.; Kim, A.V.; Koltashev, V.V.; Leuchs, G.; Motorin, S.E.; Muravyev, S.V.; Plekhovich, A.D. Development of infrared fiber lasers at 1555 nm and at 2800 nm based on Er-doped zinc-tellurite glass fiber. *J. Non-Cryst. Solids* **2019**, *525*, 119667. [[CrossRef](#)]
30. Fu, S.; Zhu, X.; Wang, J.; Wu, J.; Tong, M.; Zong, J.; Li, M.; Wiersma, K.; Chavez-Pirson, A.; Peyghambarian, N. L-band wavelength-tunable Er³⁺-doped tellurite fiber lasers. *J. Light. Technol.* **2020**, *38*, 1435–1438. [[CrossRef](#)]
31. Peng, X.; Song, F.; Jiang, S.; Peyghambarian, N.; Kuwata-Gonokami, M.; Xu, L. Fiber-taper-coupled L-band Er³⁺-doped tellurite glass microsphere laser. *Appl. Phys. Lett.* **2003**, *82*, 1497–1499. [[CrossRef](#)]
32. Peng, X.; Song, F.; Kuwata-Gonokami, M.; Jiang, S.; Peyghambarian, N. Temperature dependence of the wavelength and threshold of fiber-taper-coupled L-band Er³⁺-doped tellurite glass microsphere laser. *Appl. Phys. Lett.* **2003**, *83*, 5380–5382. [[CrossRef](#)]
33. Richards, B.; Tsang, Y.; Binks, D.; Lousteau, J.; Jha, A. Efficient ~2 μm Tm³⁺-doped tellurite fiber laser. *Opt. Lett.* **2008**, *33*, 402–404. [[CrossRef](#)]
34. Richards, B.; Tsang, Y.; Binks, D.; Lousteau, J.; Jha, A. ~2 μm Tm³⁺/Yb³⁺-doped tellurite fibre laser. *J. Mater. Sci. Mater. Electr.* **2009**, *20*, 317–320. [[CrossRef](#)]
35. Li, K.; Zhang, G.; Hu, L. Watt-level ~2 μm laser output in Tm³⁺-doped tungsten tellurite glass double-cladding fiber. *Opt. Lett.* **2010**, *35*, 4136–4138. [[CrossRef](#)]
36. Li, K.; Zhang, G.; Wang, X.; Hu, L.; Kuan, P.; Chen, D.; Wang, M. Tm³⁺ and Tm³⁺-Ho³⁺ co-doped tungsten tellurite glass single mode fiber laser. *Opt. Express* **2012**, *20*, 10115–10121. [[CrossRef](#)]
37. Jia, Z.X.; Liu, L.; Yao, C.F.; Qin, G.S.; Ohishi, Y.; Qin, W.P. Supercontinuum generation and lasing in thulium doped tellurite microstructured fibers. *J. Appl. Phys.* **2014**, *115*, 063106. [[CrossRef](#)]
38. Kuan, P.W.; Li, K.; Zhang, L.; Fan, X.; Hasan, T.; Wang, F.; Hu, L. All-Fiber Passively Q-Switched Laser Based on Tm³⁺-Doped Tellurite Fiber. *IEEE Photonics Technol. Lett.* **2015**, *27*, 689–692. [[CrossRef](#)]
39. Gao, S.; Kuan, P.W.; Liu, X.; Chen, D.; Liao, M.; Hu, L. ~2 μm Single-Mode Laser Output in Tm³⁺-Doped Tellurium Germanate Double-Cladding Fiber. *IEEE Photonics Technol. Lett.* **2015**, *27*, 1702–1704. [[CrossRef](#)]
40. Wang, S.; Yao, C.; Jia, Z.; Qin, G.; Qin, W. 1887 nm lasing in Tm³⁺-doped TeO₂-BaF₂-Y₂O₃ glass microstructured fibers. *Opt. Mater.* **2017**, *66*, 640–643. [[CrossRef](#)]
41. Sasagawa, K.; Yonezawa, Z.O.; Iwai, R.; Ohta, J.; Nunoshita, M. S-band Tm³⁺-doped tellurite glass microsphere laser via a cascade process. *Appl. Phys. Lett.* **2004**, *85*, 4325–4327. [[CrossRef](#)]
42. Wu, J.; Jiang, S.; Qua, T.; Kuwata-Gonokami, M.; Peyghambarian, N. 2 μm lasing from highly thulium doped tellurite glass microsphere. *Appl. Phys. Lett.* **2005**, *87*, 211118. [[CrossRef](#)]
43. Wu, J.; Jiang, S.; Peyghambarian, N. 1.5-μm-band thulium-doped microsphere laser originating from self-terminating transition. *Opt. Express* **2005**, *13*, 10129–10133. [[CrossRef](#)]
44. Vanier, F.; Côté, F.; El Amraoui, M.; Messaddeq, Y.; Peter, Y.A.; Rochette, M. Low-threshold lasing at 1975 nm in thulium-doped tellurite glass microspheres. *Opt. Lett.* **2015**, *40*, 5227–5230. [[CrossRef](#)]

45. Qin, J.; Huang, Y.; Liao, T.; Xu, C.; Ke, C.; Duan, Y. 1.9 μm laser and visible light emissions in $\text{Er}^{3+}/\text{Tm}^{3+}$ co-doped tellurite glass microspheres pumped by a broadband amplified spontaneous emission source. *J. Opt.* **2019**, *21*, 035401. [[CrossRef](#)]
46. Li, A.; Li, W.; Zhang, M.; Zhang, Y.; Wang, S.; Yang, A.; Yang, Z.; Lewis, E.; Brambilla, G.; Wang, P. Tm^{3+} - Ho^{3+} codoped tellurite glass microsphere laser in the 1.47 μm wavelength region. *Opt. Lett.* **2019**, *44*, 511–513. [[CrossRef](#)] [[PubMed](#)]
47. Tsang, Y.; Richards, B.; Binks, D.; Lousteau, J.; Jha, A. A $\text{Yb}^{3+}/\text{Tm}^{3+}/\text{Ho}^{3+}$ triply-doped tellurite fibre laser. *Opt. Express* **2008**, *16*, 10690–10695. [[CrossRef](#)] [[PubMed](#)]
48. Tsang, Y.; Richards, B.; Binks, D.; Lousteau, J.; Jha, A. $\text{Tm}^{3+}/\text{Ho}^{3+}$ codoped tellurite fiber laser. *Opt. Lett.* **2008**, *33*, 1282–1284. [[CrossRef](#)]
49. Yao, C.; He, C.; Jia, Z.; Wang, S.; Qin, G.; Ohishi, Y.; Qin, W. Holmium-doped fluorotellurite microstructured fibers for 2.1 μm lasing. *Opt. Lett.* **2015**, *40*, 4695–4698. [[CrossRef](#)]
50. Li, D.; Xu, W.; Kuan, P.; Li, W.; Lin, Z.; Wang, X.; Zhang, L.; Yu, C.; Li, K.; Hu, L. Spectroscopic and laser properties of Ho^{3+} doped lanthanum-tungsten-tellurite glass and fiber. *Ceram. Int.* **2016**, *42*, 10493–10497. [[CrossRef](#)]
51. Li, L.X.; Wang, W.C.; Zhang, C.F.; Yuan, J.; Zhou, B.; Zhang, Q.Y. 2.0 μm $\text{Nd}^{3+}/\text{Ho}^{3+}$ -doped tungsten tellurite fiber laser. *Opt. Mater. Express* **2016**, *6*, 2904–2914. [[CrossRef](#)]
52. Zhou, D.; Bai, X.; Zhou, H. Preparation of $\text{Ho}^{3+}/\text{Tm}^{3+}$ co-doped lanthanum tungsten germanium tellurite glass fiber and its laser performance for 2.0 μm . *Sci. Rep.* **2017**, *7*, 44747. [[CrossRef](#)]
53. Zhao, Z.P.; Yao, C.F.; Li, Z.R.; Jia, Z.X.; Qin, G.S.; Ohishi, Y.; Qin, W.P. 8.08 W holmium doped fluorotellurite fiber laser at 2067 nm. *Laser Phys. Lett.* **2019**, *16*, 115101. [[CrossRef](#)]
54. Yang, Z.; Wu, Y.; Yang, K.; Xu, P.; Zhang, W.; Dai, S.; Xu, T. Fabrication and characterization of Tm^{3+} - Ho^{3+} co-doped tellurite glass microsphere lasers operating at ~ 2.1 μm . *Opt. Mater.* **2017**, *72*, 524–528. [[CrossRef](#)]
55. Yu, J.; Wang, X.; Li, W.; Zhang, M.; Zhang, J.; Tian, K.; Du, Y.; Nic Chormaic, S.; Wang, P. An experimental and theoretical investigation of a 2 μm wavelength low-threshold microsphere laser. *J. Lightwave Technol.* **2020**, *38*. [[CrossRef](#)]
56. Li, A.; Dong, Y.; Wang, S.; Jia, S.; Brambilla, G.; Wang, P. Infrared-laser and upconversion luminescence in Ho^{3+} - Yb^{3+} codoped tellurite glass microsphere. *J. Lumin.* **2020**, *218*, 116826. [[CrossRef](#)]
57. Saffari, M.; Gholami, A.; Parsanasab, G.-M.; Firouzeh, Z.H. Investigation of a High-Power Low-Threshold Single-Mode Microsphere Laser Using a Serially Coupled Double Microsphere Structure. *J. Lightwave Technol.* **2019**, *37*, 3273–3279. [[CrossRef](#)]
58. Anashkina, E.A.; Leuchs, G.; Andrianov, A.V. Numerical simulation of multi-color laser generation in Tm -doped tellurite microsphere at 1.9, 1.5 and 2.3 microns. *Res. Phys.* **2020**, *16*, 102811. [[CrossRef](#)]
59. Anashkina, E.A.; Andrianov, A.V.; Dorofeev, V.V.; Muravyev, S.V.; Koptev, M.Y.; Sorokin, A.A.; Motorin, S.E.; Koltashev, V.V.; Galagan, B.I.; Denker, B.I. Two-color pump schemes for Er-doped tellurite fiber lasers and amplifiers at 2.7–2.8 μm . *Laser Phys. Lett.* **2019**, *16*, 025107. [[CrossRef](#)]
60. Michel, J.C.; Morin, D.; Uzel, F. Propriétés spectroscopiques et effet laser d'un verre tellurite et d'un verre phosphate fortement dopés en néodyme. *Revue Phys. Appl.* **1978**, *13*, 859–866. [[CrossRef](#)]
61. Gomes, L.; Oermann, M.; Ebdorff-Heidepriem, H.; Ottaway, D.; Monro, T.; Felipe Henriques Librantz, A.; Jackson, S.D. Energy level decay and excited state absorption processes in erbium-doped tellurite glass. *J. Appl. Phys.* **2011**, *110*, 083111. [[CrossRef](#)]
62. Oermann, M.R.; Ebdorff-Heidepriem, H.; Li, Y.; Foo, T.C.; Monro, T.M. Index matching between passive and active tellurite glasses for use in microstructured fiber lasers: Erbium doped lanthanum-tellurite glass. *Opt. Express* **2009**, *17*, 15578–15584. [[CrossRef](#)]
63. Ma, Y.; Guo, Y.; Huang, F.; Hu, L.; Zhang, J. Spectroscopic properties in Er^{3+} doped zinc-and tungsten-modified tellurite glasses for 2.7 μm laser materials. *J. Lumin.* **2014**, *147*, 372–377. [[CrossRef](#)]
64. Wang, W.C.; Yuan, J.; Li, L.X.; Chen, D.D.; Qian, Q.; Zhang, Q.Y. Broadband 2.7 μm amplified spontaneous emission of Er^{3+} doped tellurite fibers for mid-infrared laser applications. *Opt. Mater. Express* **2015**, *5*, 2964–2977. [[CrossRef](#)]
65. Chen, F.; Wei, T.; Jing, X.; Tian, Y.; Zhang, J.; Xu, S. Investigation of mid-infrared emission characteristics and energy transfer dynamics in Er^{3+} doped oxyfluoride tellurite glass. *Sci. Rep.* **2015**, *5*, 10676. [[CrossRef](#)] [[PubMed](#)]

66. Anashkina, E.A.; Dorofeev, V.V.; Muravyev, S.V.; Motorin, S.E.; Andrianov, A.V.; Sorokin, A.A.; Koptev, M.Y.; Singh, S.; Kim, A.V. Possibilities of laser amplification and measurement of the field structure of ultrashort pulses in the range of 2.7–3 μm in tellurite glass fibres doped with erbium ions. *Quantum Electron.* **2018**, *48*, 1118–1127. [CrossRef]
67. Denker, B.I.; Dorofeev, V.V.; Galagan, B.I.; Koltashev, V.V.; Motorin, S.E.; Sverchkov, S.E.; Plotnichenko, V.G. Rare-earth ions doped zinc-tellurite glass for 2–3 μm lasers. *Appl. Phys. B* **2018**, *124*, 235. [CrossRef]
68. Aydin, Y.O.; Fortin, V.; Maes, F.; Jobin, F.; Jackson, S.D.; Vallée, R.; Bernier, M. Diode-pumped mid-infrared fiber laser with 50% slope efficiency. *Optica* **2017**, *4*, 235–238. [CrossRef]
69. Sujecki, S.; Sojka, L.; Seddon, A.B.; Benson, T.M.; Barney, E.; Falconi, M.C.; Prudeniano, F.; Marciniak, M.; Baghdasaryan, H.; Peterka, P.; et al. Comparative modeling of infrared fiber lasers. *Photonics* **2018**, *5*, 48. [CrossRef]
70. Cajzl, J.; Peterka, P.; Kowalczyk, M.; Tarka, J.; Sobon, G.; Sotor, J.; Aubrecht, J.; Honzátko, P.; Kašík, I. Thulium-doped silica fibers with enhanced fluorescence lifetime and their application in ultrafast fiber lasers. *Fibers* **2018**, *6*, 66. [CrossRef]
71. Sujecki, S. Modeling and design of lanthanide ion-doped chalcogenide fiber lasers: Progress towards the Practical realization of the first MIR chalcogenide fiber laser. *Fibers* **2018**, *6*, 25. [CrossRef]
72. Anashkina, E.A.; Kim, A.V. Numerical simulation of ultrashort mid-IR pulse amplification in praseodymium doped chalcogenide fibers. *J. Lightwave Technol.* **2017**, *35*, 5397–5403. [CrossRef]
73. Andrianov, A.; Szabo, A.; Sergeev, A.; Kim, A.; Chvykov, V.; Kalashnikov, M. Computationally efficient method for Fourier transform of highly chirped pulses for laser and parametric amplifier modeling. *Opt. Express* **2016**, *24*, 25974–25982. [CrossRef]
74. Gomes, L.; Lousteau, J.; Milanese, D.; Scarpignato, G.C.; Jackson, S.D. Energy transfer and energy level decay processes in Tm³⁺-doped tellurite glass. *J. Appl. Phys.* **2012**, *111*, 063105. [CrossRef]
75. Ng, L.N.; Taylor, E.R.; Nilsson, J. 795 nm and 1064 nm dual pump thulium-doped tellurite fibre for S-band amplification. *Electron. Lett.* **2002**, *38*, 1246–1247. [CrossRef]
76. Taylor, E.R.M.; Ng, L.N.; Nilsson, J.; Caponi, R.; Pagano, A.; Potenza, M.; Sordo, B. Thulium-doped tellurite fiber amplifier. *IEEE Photonics Technol. Lett.* **2004**, *16*, 777–779. [CrossRef]
77. Caponi, R.; Pagano, A.; Potenza, M.; Sordo, B.; Taylor, E.M.; Ng, L.N.; Nilsson, J.; Poli, F. Nearly 10 dB net gain from a thulium-doped tellurite fibre amplifier over the S-band. In Proceedings of the 29th European Conference on Optical Communication—14th International Conference on Integrated Optics and Optical Fibre Communication (ECOC-IOOC 2003), Rimini, Italy, 21–25 September 2003.
78. Venkataiah, G.; Babu, P.; Martín, I.R.; Krishnaiah, K.V.; Suresh, K.; Lavín, V.; Jayasankar, C.K. Spectroscopic studies on Yb³⁺-doped tungsten-tellurite glasses for laser applications. *J. Non-Cryst. Solids* **2018**, *479*, 9–15. [CrossRef]
79. Merzliakov, M.A.; Kouhar, V.V.; Malashkevich, G.E.; Pestryakov, E.V. Spectroscopy of Yb-doped tungsten-tellurite glass and assessment of its lasing properties. *Opt. Mater.* **2018**, *75*, 142–149. [CrossRef]
80. Babu, A.M.; Jamalaiah, B.C.; Kumar, J.S.; Sasikala, T.; Moorthy, L.R. Spectroscopic and photoluminescence properties of Dy³⁺-doped lead tungsten tellurite glasses for laser materials. *J. Alloys Compd.* **2011**, *509*, 457–462. [CrossRef]
81. Giridhar, P.; Sailaja, S.; Reddy, B.M.; Raju, V.K.; Raju, N.C.; Reddy, S.B. Spectroscopic studies of RE³⁺ (RE = Eu, Tb, Sm & Dy): Lithium lead boro tellurite glasses. *Ferroelectr. Lett.* **2011**, *38*, 1–10. [CrossRef]
82. Annapurna, K.; Chakrabarti, R.; Buddhudu, S. Absorption and emission spectral analysis of Pr³⁺: Tellurite glasses. *J. Mater. Sci.* **2007**, *42*, 6755–6761. [CrossRef]
83. Marek, Ł.; Sobczyk, M. Spectroscopic investigations of Pr³⁺ ions in Na₂O-La₂O₃-ZnO-TeO₂ glasses. *J. Non-Cryst. Solids* **2018**, *487*, 96–103. [CrossRef]
84. Stambouli, W.; Elhouichet, H.; Gelloz, B.; Férid, M. Optical and spectroscopic properties of Eu-doped tellurite glasses and glass ceramics. *J. Lumin.* **2016**, *138*, 201–208. [CrossRef]
85. Alvarez-Ramos, M.E.; Alvarado-Rivera, J.; Zayas, M.E.; Caldiño, U.; Hernández-Paredes, J. Yellow to orange-reddish glass phosphors: Sm³⁺, Tb³⁺ and Sm³⁺/Tb³⁺ in zinc tellurite-germanate glasses. *Opt. Mater.* **2018**, *75*, 88–93. [CrossRef]
86. Kumar, A.; Rai, D.K.; Rai, S.B. Optical properties of Sm³⁺ ions doped in tellurite glass. *Spectrochim. Acta Part A Mol. Biomol. Spectrosc.* **2003**, *59*, 917–925. [CrossRef]

